Operation Mode Analysis and Peak Gain Approximation of the LLC Resonant Converter

Xiang Fang, *Student Member, IEEE*, Haibing Hu, *Member, IEEE*, Z. John Shen, *Fellow, IEEE*, and Issa Batarseh, *Fellow, IEEE*

***Abstract*—With the advantage of achieving zero voltage switching for a wide input voltage range, the LLC resonant topology has become increasingly popular for use in high power density and high-efficiency power converter applications. However, when the LLC converter is applied to wide input voltage range applications, the widely used fundamental harmonic approximation is incapable of guiding the design due to its inaccuracy. Thus an accurate LLC converter model is desired. In this paper, a generalized mode analysis is presented that provides highly accurate prediction on resonant current and voltage behavior and dc gain characteristic. Also, because operation modes are affected by load, frequency, and gain conditions, the boundaries and distribution of modes are discussed and illustrated. Based on the mode analysis, an approximation method is developed to estimate the peak gain point, which is useful in LLC design. This approximation demonstrates high accuracy within the simulation results. An experimental prototype is built to verify the analysis.**

***Index Terms*—DC–DC power conversion, generalized analysis, resonant converter.**

I. Introduction

THE development of power supply technology demands high efficiency and high power density in power conversion. The LLC resonant converter is recognized as a feasible topology to meet this trend and has become popular in various switching-mode power supply applications [1]–[5]. This converter has the advantage of achieving zero voltage switching (ZVS) for a wide input voltage and load range, which allows the converter to operate in high frequency without compromising efficiency for switching losses and, therefore, reduces component sizes and increases power density. As shown in Fig. 1, the LLC topology is similar to *L–C* series resonant converter (SRC) but with a shunt inductor L_m paralleled to the transformer. By introducing the third resonant component, it overcomes SRC's regulation issues under light-load condition, improves the power efficiency, and allows the converter to operate in boost mode (voltage gain >1). In addition, the added inductor can be integrated with the transformer as the magnetizing inductance at no extra cost. However, the LLC topology is difficult to analyze because of its multiple resonant components and various operation modes [6].

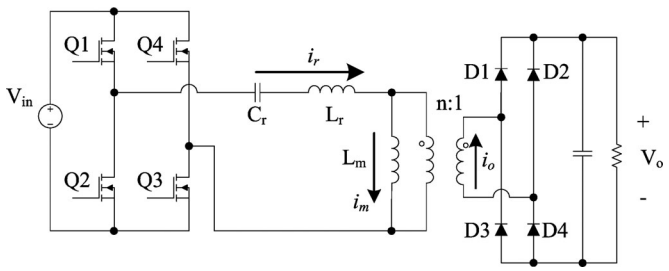

Fig. 1. Full-bridge LLC resonant converter.

Fundamental harmonic approximation (FHA) [7], [8] is a widely used method in resonant converter analysis, which treats the current and voltage waveforms as pure sinusoids at the fundamental frequency and neglects other high-order harmonics. Although FHA provides a straightforward method for calculating the dc gain, the accuracy drops when the switching frequency moves away from the resonant frequency as the current/voltage waveforms become more nonsinusoidal. FHA can be improved by taking high-order distortion into account [9], [10] or including parasitic components in the analysis [11], but this will become cumbersome in practical use. Moreover, harmonic analysis methods fail to reveal various operation modes of the LLC converter. Another approach is to use state-space analysis, which can provide an accurate description of voltage and current waveforms [12]–[16]. However, it is complicated and difficult to interpret and use. Some studies on operation modes can be found in [17] and [18], however the discussion is more focused on explaining the resonant current and voltage behavior under different modes rather than predicting the dc gain, and the mode relation is not thoroughly addressed. An accurate dc gain characteristic is more useful in guiding the design than is an accurately described current and voltage behaviors.

A generalized analysis of the operation modes of the LLC converter is presented in this paper. Since the circuit behavior in one switching cycle can be divided into several stages based on different resonant conditions, the operation modes can be characterized as having different sets of stages. Through analysis and simulation, six major operation modes are found, and each mode has its own boundary conditions that can be used to solve for the dc gain and voltage and current waveforms. Operating in what given mode is determined by the switching frequency and load condition. Previous studies have only given a general description of the mode distribution and the analysis of the

Manuscript received June 30, 2011; revised September 6, 2011; accepted September 8, 2011. Date of current version February 20, 2012. Recommended for publication by Associate Editor C. K. Tse.

X. Fang, Z. J. Shen, and I. Batarseh are with the Department of Electrical Engineering and Computer Science, University of Central Florida, Orlando, FL 32826 USA (e-mail: fangx03@gmail.com; johnshen@mail.ucf.edu; batarseh@mail.ucf.edu).

H. Hu is with the Department of Electrical Engineering and Computer Science, University of Central Florida, Orlando, FL 32826 USA, and also with Nanjing University of Aeronautics and Astronautics, Nanjing 210016, China (e-mail: huhaibingucf@gmail.com).

Digital Object Identifier 10.1109/TPEL.2011.2168545

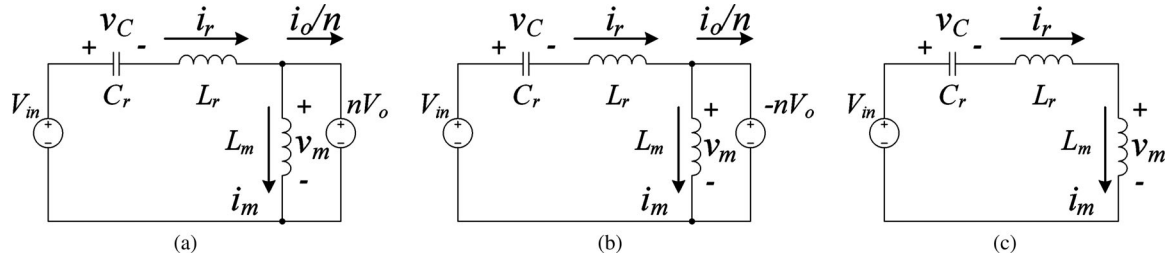

Fig. 2. LLC resonant tank equivalent circuits in half switching cycle. (a) Stage P. (b) Stage N. (c) Stage O.

mode boundaries is incomplete or based on approximations [17]–[20]. In this paper, we explore the boundaries between the six major modes, and analyze the mode distribution under different conditions.

It is found from the mode analysis that the gain has closed-form solutions if the LLC is operating under continuous conduction mode (CCM). In CCM the current released to the secondary side is continuous, while the gain prediction in discontinuous conduction mode (DCM) involves nonlinear equation solving, which is difficult and time-consuming and requires using numerical computing software. To avoid the complexity in solving the full-voltage gain characteristic curve, we focus on the peak gain points instead. In the design procedure of the LLC converter [3], [21], [22], the peak voltage gain is a key design parameter as it indicates the converter's capability in voltage regulation, which determines the minimum input voltage. The switching frequency at the peak gain is the lowest permissible operating frequency, as the slope of the gain–frequency curve is reverse to positive below the peak, which will make the control loop unstable. Also, the LLC converter should operate above the frequency of the peak gain to remain in ZVS, since the peak gain is the boundary between ZVS and ZCS regions [1], [16]. As previously mentioned, many methods have been proposed to improve gain prediction accuracy or simplify the calculation, but there is no direct method to evaluate the peak gain without using simulation tools or graphical method. This paper proposes a numerical approximation method that provides accurate peak gain prediction based on mode analysis. The approximation method gives not only the peak gain value as a function of the switching frequency but also the corresponding load power, which can be conveniently employed to facilitate the converter design. The estimated results agree well with simulations. An experimental prototype is built to verify the analysis.

II. Resonant Stage Analysis

The complexity of LLC operation is due to its dual resonant mechanism that, besides resonance formed by L_r and C_r, L_m can join the resonant tank when the secondary-side rectifiers are all OFF. The converter can operate in multiple resonant stages within one switching cycle depending on the circuit specification, switching frequency, and load conditions. In the half switching cycle when Q1, Q3 turn ON and Q2, Q4 turn OFF (see Fig. 1), there are three possible resonant stages for the resonant tank, which can be characterized by L_m voltage condition: positive clamped stage $v_m = nV_O$ (stage P), negative clamped stage $v_m = -nV_O$ (stage N), and freewheeling stage $|v_m| \le nV_O$ (stage O), where n is the transformer turns ratio. The resonant tank equivalent circuit of the three stages is given in Fig. 2. Since the LLC converter uses variable frequency control to regulate the voltage and the switching duty cycle is fixed to 50% [1], the resonant tank current and voltage waveforms of one half cycle are symmetrical to the other half in reverse direction or polarity. The following discussion focuses on the half cycle when Q1, Q3 turn ON and Q2, Q4 turn OFF. To generalize the analysis, normalized variables are used in the equations and expressions throughout the paper, which are defined as follows:

$$\text{normalized switching frequency: } f_n = f_s/f_r$$

$$\text{normalized voltage variable: } v_n = v/(nV_o)$$

$$\text{normalized current variable: } i_n = i/(nV_o/Z_r)$$

$$\text{normalized load power: } p_{on} = P_o/(n^2V_o^2/Z_r)$$

where $f_r = 1/(2\pi\sqrt{L_rC_r})$ and $Z_r = \sqrt{L_r/C_r}$.

In stage P, since L_m is clamped to nV_O, i_m increases linearly. L_r and C_r are in resonance and i_r waveform is sinusoidal. The secondary-side rectifiers conduct through D1 and D4. The normalized inductor currents i_r and i_m and capacitor voltage v_C can be described as follows:

$$\begin{aligned} i_{rPn}(\theta) &= I_{rPn}\sin(\theta+\theta_{P0}) \\ i_{mPn}(\theta) &= I_{mPn} + \theta/(m-1) \\ v_{CPn}(\theta) &= -I_{rPn}\cos(\theta+\theta_{P0}) - 1 + 1/M \end{aligned} \tag{1}$$

where

$$\theta = 2\pi f_r t, \quad m = (L_m + L_r)/L_r, \quad M = nV_o/V_{\text{in}}$$

I_{rPn} is the normalized magnitude of the sinusoidal L_r current in stage P, θ_{P0} is the initial phase angle of i_{rPn}, and I_{mPn} is the initial L_m current when stage P starts. As the current through D1 and D4 is restrained in one direction, it requires that $i_{rPn} > i_{mPn}$ in stage P.

Stage N is similar to stage P as L_m does not join the resonance of L_r and C_r, but v_m is clamped to $-nV_O$ rather than nV_O. The magnetizing current i_m is decreasing linearly, D1 and D4 are OFF, and D2 and D3 are conducting. The resonant current and voltage can be expressed as

$$\begin{aligned} i_{rNn}(\theta) &= I_{rNn}\sin(\theta+\theta_{N0}) \\ i_{mNn}(\theta) &= I_{mNn} - \theta/(m-1) \\ v_{CNn}(\theta) &= -I_{rNn}\cos(\theta+\theta_{N0}) + 1 + 1/M \end{aligned} \tag{2}$$

where I_{rNn} and I_{mNn} are the normalized current parameters, and θ_{N0} is the initial phase angle of i_{rNn}. The current constraint of this stage is $i_{rNn} < i_{mNn}$.

For stage O, L_m joins the resonance with L_r and C_r, the rectifier diodes are turned OFF, and thus no current flows to the output. Hence, i_r and i_m are equal and in pure sinusoidal waveform, the resonant frequency becomes $f_r/\sqrt{m}$. The expressions of the resonant variables are given by

$$\begin{aligned} i_{rOn}(\theta) &= i_{mOn}(\theta) = I_{rOn}\sin(\theta/\sqrt{m}+\theta_{O0}) \\ v_{COn}(\theta) &= -\sqrt{m}I_{rOn}\cos(\theta/\sqrt{m}+\theta_{O0})+1/M \\ v_{mOn}(\theta) &= \frac{m-1}{\sqrt{m}}I_{rOn}\cos(\theta/\sqrt{m}+\theta_{O0}) \end{aligned} \tag{3}$$

where I_{rOn} is the normalized current parameter and θ_{O0} is the initial phase angle. The constraint condition of stage O is that $|v_m|$ should be less than nV_O to avoid turning ON rectifier diodes.

III. Operation Mode Analysis

Different sequential combinations of the three stages in half switching cycle (in which Q1, Q3 are ON) form various operation modes of the LLC converter, which can, therefore, be used to denote the modes. For example, PO mode indicates that the resonant tank first operates in stage P and then enters stage O during the half cycle. In general, there are six major operation modes: PO, PON, PN, NP, NOP, and OPO [18]. Although some other modes exist in a low-frequency (usually below$f_r/\sqrt{m}$) region, which might have more than three stages in one half cycle, they are not discussed in this paper since they are in ZCS region and normally the LLC converter is designed to operate in ZVS region for power efficiency considerations [1].

Each operation mode is constrained by the boundary conditions at the joints of adjacent stages and at the switching instants. As the capacitor voltage and inductor current should maintain their continuity between two stages, if we use X, Y to denote two different adjacent stages, the continuity conditions can be expressed by

$$\begin{aligned} i_{rXn}(\theta_X) &= i_{rYn}(0) \\ i_{mXn}(\theta_X) &= i_{mYn}(0) \\ v_{CXn}(\theta_X) &= v_{CYn}(0). \end{aligned} \tag{4}$$

In addition, if X is stage O, stage O constraint requires that the absolute value of the voltage across L_m should be less than nV_o, $|v_m| \le nV_o$, but in stage P or N v_m is clamped by the output voltage. Thus, the constraint for v_m at the end of stage O is given by

$$v_{mOn}(\theta_O) = \begin{cases} 1, & \text{followed by stage P} \\ -1, & \text{followed by stage N.} \end{cases} \tag{5}$$

If X is stage P or N, the inductor current constraint, which is that i_r should be larger or smaller than i_m for the entire stage, will be altered when entering stage Y. Thus, i_r and i_m are equal at the end of stage X, which give the constraint condition that

$$i_{rXn}(\theta_X) = i_{mXn}(\theta_X). \tag{6}$$

Note that if Y is stage O, as i_r is equal to i_m in stage O, (6) is already included in (4).

By symmetry, the end values of i_r, i_m, and v_C should be opposite to their initial values in steady state. If we use X to denote the start stage and Y to denote the end stage in a half cycle, the symmetry conditions are given by

$$\begin{aligned} i_{rXn}(0) &= -i_{rYn}(\theta_Y) \\ i_{mXn}(0) &= -i_{mYn}(\theta_Y) \\ v_{CXn}(0) &= -v_{CYn}(\theta_Y). \end{aligned} \tag{7}$$

Since the output current is discontinued in stage O, only stages P and N are involved in the energy delivery. Thus, the normalized output power can be expressed as

$$p_{on} = \frac{f_n}{\pi}\left[\int_0^{\theta_P}(i_{rPn}-i_{mPn})d\theta + \int_0^{\theta_N}(i_{mNn}-i_{rNn})d\theta\right] \tag{8}$$

where θ_P and θ_N represent the length of stages P and N. Note that π/f_n ($=\pi f_r/f_s$) is the half cycle period in phase angle term.

Applying (4)–(8) properly to an operation mode as the boundary conditions and taking p_{on}, f_n, and m as known parameters, we can find sufficient equations to solve for the voltage gain M and other current and voltage variables. Since i_m waveform is sinusoidal in stage O and linear in stage P or N, the boundary equation about i_m in (5) will lead to a transcendental equation if a mode contains stage O. Hence, all DCMs, PO, PON, NOP, and OPO, have no closed-form solutions and rely on numerical calculation tools to solve the mode equations, whereas the CCMs, PN and NP, can be solved analytically. The current and voltage waveforms for each mode are given in Fig. 3, whereas the gain characteristic plots are given in Fig. 4.

A. PO Mode

As shown in Fig. 3(a), starting with stage P currents i_r and i_m have the same negative initial value and then they diverge in different wave shapes. Current i_m increases linearly as L_m is clamped to $+nV_o$, while i_r varies sinusoidally as L_r and C_r are in resonance. When i_r and i_m converge at the end of stage P, the rectifier diodes are both turned OFF and the LLC moves to stage O. In stage O, v_m decreases sinusoidally but is always above $-nV_o$, otherwise the resonant tank will enter stage N within the half cycle.

It can be seen from Fig. 4(a) that the gain M in PO mode increases monotonically with the decrease of f_n, and gain curves for various loads converge to 1 at $f_n = 1$. In other words, the peak gains do not occur in this mode and the entire mode is within ZVS region. In addition, the slope of the gain–frequency curves in PO mode is always negative, which ensures the control stability in the closed-loop design. Therefore, PO mode is the preferable operation mode of the LLC converter.

B. PON Mode

By increasing the load or decreasing the switching frequency, the converter may change from PO mode to PON mode as shown in Fig. 3(b). Although the first two stages of PON mode are the

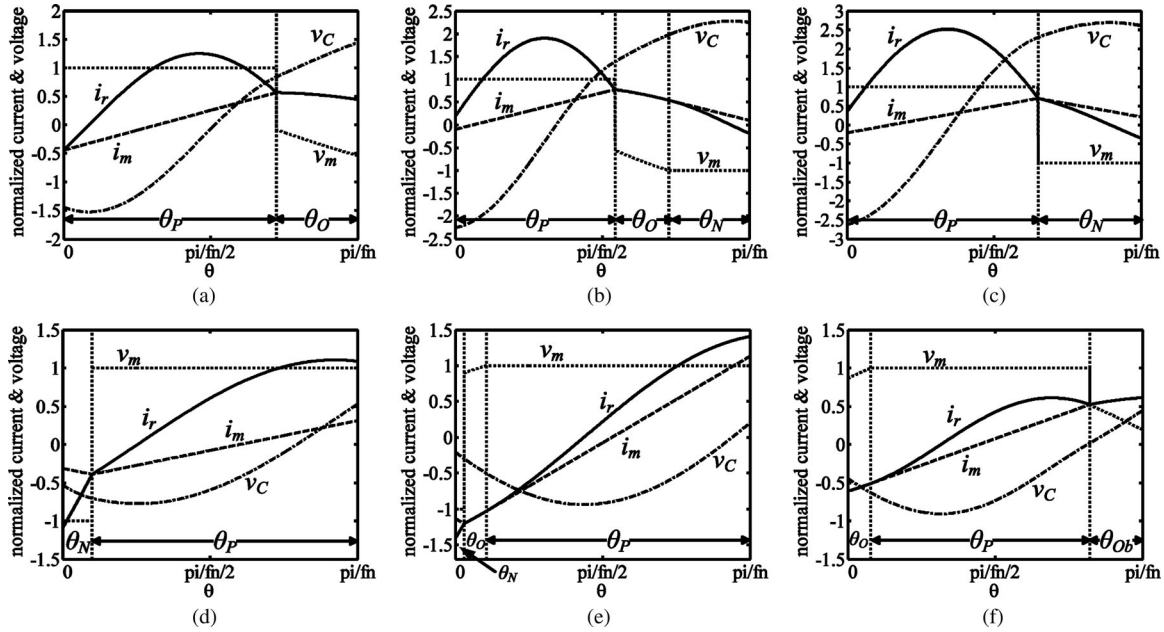

Fig. 3. Typical LLC operation modes waveforms. (a) PO mode with $m = 4, p_{on} = 0.5, f_n = 0.75$. (b) PON mode with $m = 4, p_{on} = 0.6, f_n = 0.65$. (c) PN mode with $m = 4, p_{on} = 1.1, f_n = 0.75$. (d) NP mode with $m = 4, p_{on} = 0.6, f_n = 1.34$. (e) NOP mode with $m = 2, p_{on} = 0.25, f_n = 1.3$. (f) OPO mode with $m = 4, p_{on} = 0.15, f_n = 0.75$.

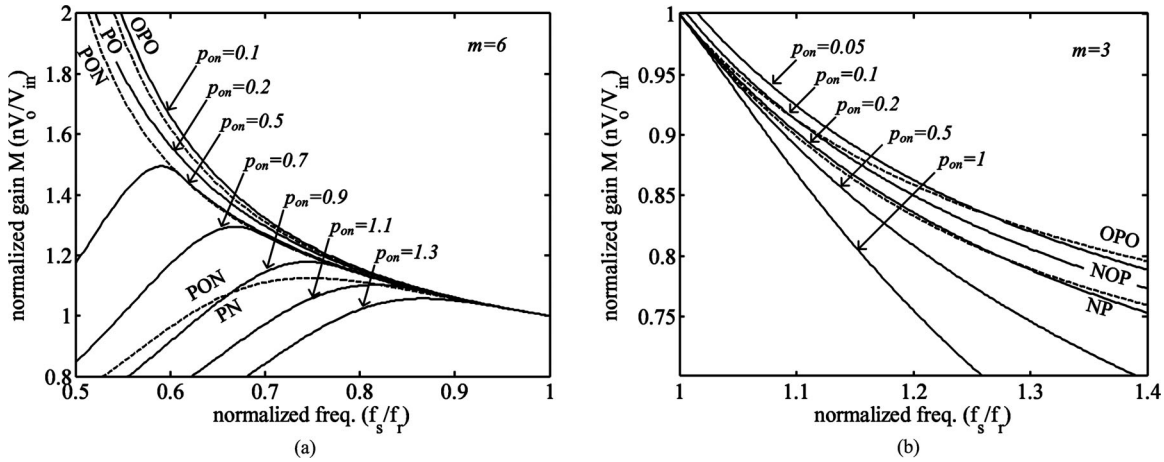

Fig. 4. Normalized gain M curves (solid lines) of the LLC converter for various load conditions in different modes. (Mode boundaries are marked by the dashed lines.)

same as PO mode, i_r and i_m in PON start with different initial current at the start. When stage O ends, L_m voltage falls down to $-nV_o$, diodes D2 and D3 are turned ON and L_m is clamped to $-nV_o$, which starts stage N. The resonant tank current i_r in stage N varies sinusoidally below i_m. Before i_r and i_m converge again, the half switching cycle ends with Q1, Q3 turned OFF. Since the output current is not zero at the switching instants, the secondary-side diodes have reverse recovery losses. For a certain p_{on}, the gain–frequency relation is no longer monotonic and a gain curve may reach its peak and fall below 1 in this mode [see Fig. 4(a)]. The converter should avoid operating below the frequency of peak gain as it is in the ZCS region and could cause control instability.

C. PN Mode

The stage O of PON mode is shortened if the converter load increases. When the length of stage O shrinks to 0, the LLC enters PN mode as shown in Fig. 3(c). L_m does not have the resonant stage and i_m varies as a triangle waveform. The boundary conditions can be obtained from (4), (6)–(8) as

$$I_{rPn}\sin(\theta_P + \theta_{P0}) - I_{rNn}\sin(\theta_{N0}) = 0$$
$$I_{rPn}\cos(\theta_P + \theta_{P0}) - I_{rNn}\cos(\theta_{N0}) + 2 = 0$$
$$I_{rPn}\sin(\theta_{P0}) + I_{rNn}\sin(\theta_N + \theta_{N0}) = 0$$
$$I_{rPn}\sin(\theta_P + \theta_{P0}) + I_{rNn}\sin(\theta_{N0}) - \pi/[f_n(m-1)] = 0$$
$$I_{rPn}\cos(\theta_{P0}) + I_{rNn}\cos(\theta_N + \theta_{N0}) - 2/M = 0$$

$$I_{rNn}\cos(\theta_{N0}) - 1 - 1/M + p_{on}\pi/(2f_n) = 0. \quad (9)$$

Note that $\theta_P + \theta_N = \pi/f_n$. After proper manipulation, we arrive at the following equations:

$$\sin\theta_P = \frac{M}{2}\frac{\pi}{(m-1)f_n}\cos\left(\frac{\pi}{2f_n}\right) \times\left[\cos\left(\frac{\pi}{2f_n}\right) + \sin\left(\frac{\pi}{2f_n}\right)\cot\theta_{N0}\right]$$

$$\cos\theta_P = \frac{M}{2}\frac{\pi}{(m-1)f_n}\cos\left(\frac{\pi}{2f_n}\right) \times\left[\cos\left(\frac{\pi}{2f_n}\right)\cot\theta_{N0} - \sin\left(\frac{\pi}{2f_n}\right)\right] - M \quad (10)$$

where

$$\cot\theta_{N0} = \left(2 + \frac{2}{M} - p_{on}\frac{\pi}{f_n}\right)\Big/\frac{\pi}{(m-1)f_n}.$$

By substituting (10) into $\sin^2\theta_P + \cos^2\theta_P = 1$, it yields a quadratic polynomial equation about M, given f_n and p_{on} as known parameters. Hence, closed-form solutions for PN mode can be found. As shown in Fig. 4(a), the dc gain in PN mode is lower than in PON or PO mode at the same switching frequency.

D. NP Mode

NP mode [see Fig. 3(d)] occurs when the switching frequency is above resonant frequency f_r. For this mode, the LLC has not enough time to finish stage P and enter another stage before the half cycle ends. The current i_r is higher than i_m when stage P ends, and the symmetry requires that i_r is lower than i_m at the start of the half cycle which means that it begins with stage N. The mode equations of NP mode are similar to PN mode as the two stages are the same but in reverse order. Similar to PN mode, the following equations can be used to derive the explicit expression of dc gain

$$\sin\theta_N = \frac{M}{2}\frac{\pi}{(m-1)f_n}\cos\left(\frac{\pi}{2f_n}\right) \times\left[\cos\left(\frac{\pi}{2f_n}\right) + \sin\left(\frac{\pi}{2f_n}\right)\cot\theta_{P0}\right]$$

$$\cos\theta_N = \frac{M}{2}\frac{\pi}{(m-1)f_n}\cos\left(\frac{\pi}{2f_n}\right) \times\left[\cos\left(\frac{\pi}{2f_n}\right)\cot\theta_{P0} - \sin\left(\frac{\pi}{2f_n}\right)\right] + M \quad (11)$$

where

$$\cot\theta_{P0} = \left(-2 + \frac{2}{M} + p_{on}\frac{\pi}{f_n}\right)\Big/\frac{\pi}{(m-1)f_n}.$$

The voltage gain M of this mode is lower than 1 and decreases as f_n increases [see Fig. 4(b)]. Although the gain–frequency relation is also monotonic as in PO mode, NP mode has additional diode reverse recovery losses compared to PO mode. Therefore, in order to reduce the power losses, we could limit the switching frequency below f_r to avoid NP mode.

E. NOP Mode

NOP mode also occurs in $f_n > 1$ region as NP mode but it is for lighter load conditions. It has an additional cutoff stage O between stages N and P [see Fig. 3(e)] compared to NP mode. This is because at the end of stage N, the L_m voltage is not high enough ($v_m < nV_o$) to immediately turn ON D1 and D4. After gaining sufficient voltage increase in stage O, L_m will be clamped by output through D1 and D4, and then the resonant tank enters stage P. Similar to NP mode, the gain in NOP mode decreases with the increase of f_n.

F. OPO Mode

OPO mode [see Fig. 3(f)] exits under light-load condition. At the start of the half switching cycle, v_m is not high enough to start stage P, and thus the LLC operates in stage O. And after stage P, v_m is not low enough to start stage N, and thus this mode ends up in stage O as well. OPO mode has relatively higher gain than other modes and exists for a frequency range from below to above f_r (see Fig. 4).

IV. Mode Boundaries and Distribution

Different operation modes of the LLC converter have different load, gain, and frequency distribution. Therefore, in order to obtain a complete voltage gain curve, knowing the boundaries and distribution of modes is essential in order to apply the appropriate mode equations according to the load and frequency conditions. The mode edges could be a special case of one of the six operation modes or a particular boundary mode. In addition to the six major modes, there are three boundary modes that only occur at the boundaries between the six modes, which are O mode under zero-load condition, P mode at resonant frequency f_r, and OP mode at the boundary between NOP and OPO modes. Fig. 5 shows the distribution of the operation modes in a range of switching frequency, load power, and gain, which is generated by solving boundary mode equations using MATLAB.

PO, PON, and PN modes can only be found in the region below resonant frequency f_r. PO and PON both contain stage O and, therefore, are operating under DCM, whereas PN is in CCM and has relatively heavier load condition. For the same switching frequency, the dc gain relation between these three modes is that PO > PON > PN [see Fig. 5(a)]. The boundary mode of PO and PON is PO mode. In the boundary PO mode, the end v_m value in stage O is $-nV_o$, and exceeding this lower limit will lead the converter to stage N. If v_m reaches $-nV_o$ before the half cycle finishes, the LLC would start to operate in PON mode. Thus, the boundary condition is given by

$$v_{mOn}(\theta_O) = -1. \quad (12)$$

With (12), applying (4), (7) as the PO boundary conditions is enough to solve the gain and voltage/current variables without knowing p_{on} and using the load condition equation (8). In other words, the load power p_{on} and gain M of OP mode is uniquely determined by m and f_n.

The boundary mode between PON and PN is PN mode. For PN mode, it requires that the initial v_m of stage N is low enough

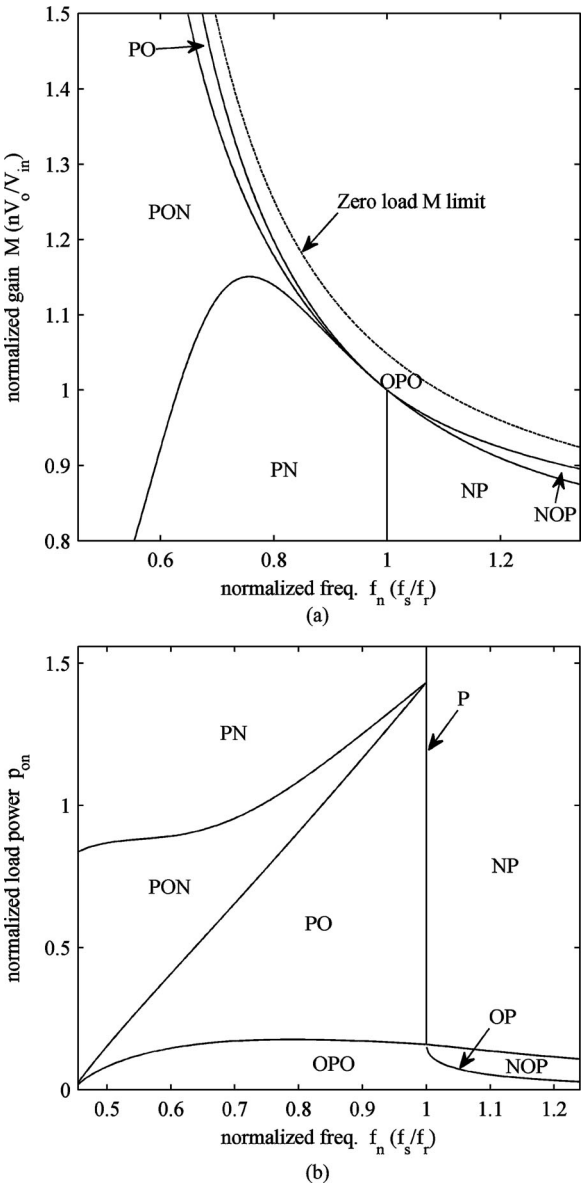

Fig. 5. LLC mode boundaries and distribution with $m = 5$. (a) Gain–frequency distribution and the zero-load gain limit (the dashed line). (b) Load-frequency distribution.

($v_m \leq -nV_o$) to turn ON D2 and D3 so that the converter can directly enter stage N after stage P without the transition of stage O. Therefore, in boundary PN mode the initial v_m of stage N should be equal to $-nV_o$, and since i_m and i_r are equal at the start of stage N, this boundary constraint can be expressed as

$$(m-1)\frac{di_{rNn}(0)}{d\theta} = (m-1)I_{rNn}\cos(\theta_{N0}) = -1. \quad (13)$$

Combining (13) with (9), the gain and load expressions can be solved as shown by (14), at the bottom of this page.

NP and NOP modes occur above resonant frequency ($f_n > 1$) and NP is for heavier load condition than NOP. Their boundary mode is NP mode. In NP mode, the instant v_m value at the start of stage P should be larger than nV_o to let L_m clamp the output. Therefore, the boundary condition at the edge of NP mode to NOP mode is

$$(m-1)\frac{di_{rPn}(0)}{d\theta} = (m-1)I_{rPn}\cos(\theta_{P0}) = 1. \quad (15)$$

Similarly, the gain and load expressions on the mode boundary can be derived as shown in (16), at the bottom of this page.

The operation frequency of OPO mode spans from below to above the resonant point. For $f_n < 1$, OPO mode borders with PO mode. The boundary mode is PO mode, and (15) applies as the additional constraint condition. For $f_n > 1$, OPO mode borders with NOP mode, and their boundary is OP mode. Boundary equations (4) and (7) apply to both OP and PO modes, but (5) only applies to OP mode. Hence, OP mode has one more constraint condition than PO mode and OP mode can be solved without knowing p_{on}.

At resonant frequency ($f_n = 1$), stage P will dominate the whole half cycle while stage O or N vanishes, which forms the boundary P mode. In P mode, as $\theta_P = \pi$, i_r, and v_C are pure sinusoidal and i_m is a triangle waveform. From the symmetry

$$M = \frac{m-1}{\sqrt{m^2 - 2m\sin\left(\frac{\pi}{2f_n}\right)\left(\sin\left(\frac{\pi}{2f_n}\right) - \frac{\pi}{2f_n}\cos\left(\frac{\pi}{2f_n}\right)\right) + \left(\sin\left(\frac{\pi}{2f_n}\right) - \frac{\pi}{2f_n}\cos\left(\frac{\pi}{2f_n}\right)\right)^2}}$$
$$p_{on} = \frac{2f_n}{\pi}\left[1 + \frac{1}{M} + \frac{1}{m-1}\right]. \quad (14)$$

$$M = \frac{m-1}{\sqrt{m^2 - 2m\sin\left(\frac{\pi}{2f_n}\right)\left(\sin\left(\frac{\pi}{2f_n}\right) + \frac{\pi}{2f_n}\cos\left(\frac{\pi}{2f_n}\right)\right) + \left(\sin\left(\frac{\pi}{2f_n}\right) + \frac{\pi}{2f_n}\cos\left(\frac{\pi}{2f_n}\right)\right)^2}}$$
$$p_{on} = \frac{2f_n}{\pi}\left[1 - \frac{1}{M} + \frac{1}{m-1}\right]. \quad (16)$$

conditions (7), we have

$$I_{mPn} = -\frac{\pi}{2(m-1)}$$
$$M = 1. \tag{17}$$

Hence, the normalized dc gain is always equal to 1 in P mode. Because the unity gain is load independent, the LLC converters are often designed to work at resonance for normal input voltage to narrow the operating frequency range [23]. However, under light-load condition, it may operate in OPO mode even at resonant frequency and the gain is slightly larger than 1 [see Fig. 5(a)]. At the edge of P mode to OPO mode, the boundary condition can also be described by (15). Substituting (15) and $f_n = 1$ into (8) gives the boundary load power expression as

$$p_{on} = \frac{2}{\pi} I_{rPn} \cos(\theta_{P0}) = \frac{2}{\pi(m-1)}. \tag{18}$$

If the load is lighter than the boundary, the LLC will be operated in OPO mode.

As f_n approaches 1, θ_P approaches π, and θ_O approaches 0, the limit of load power p_{on} of OP mode is the same as (18) defined. Since the PO/OPO and NP/NOP boundary condition (15) also leads to (18) at $f_n = 1$, the boundaries between OPO, PO, NOP, and NP all converge to the same load point defined by (18).

Also, it is observed that as f_n approaches 1, the boundaries between PO, PON, and PN mode converge to one load point at resonant frequency, at which the normalized load power can be derived from (12), (13), and (8) as

$$p_{on} = \frac{2}{\pi} \frac{2m-1}{m-1}. \tag{19}$$

If the load drops to zero, the converter will operate in O mode. In this mode, no power flows to the output that there is no stage P nor N, and all energy is circulating in the primary-side resonant tank. Ideally, input voltage can be arbitrarily small since the output voltage held up by the output capacitor is cut off from input. However, there is limitation on the maximum value of V_{in}. To prevent turning on secondary-side diodes, L_m voltage should not exceed nV_o or $-nV_o$ ($|v_m| \le nV_o$), which is given by

$$v_{mOn}(\theta) = \frac{m-1}{\sqrt{m}} I_{rOn} \cos(\theta/\sqrt{m} + \theta_{O0}) \le \frac{m-1}{\sqrt{m}} I_{rOn} \le 1. \tag{20}$$

From the symmetry condition (7), we can derive that

$$\sqrt{m} I_{rOn} \cos\left(\frac{\pi}{2f_n\sqrt{m}}\right) = \frac{1}{M}. \tag{21}$$

After combining (20) and (21), the gain limit [see Fig. 5(a)] can be expressed as

$$M \ge \frac{m-1}{m\cos[\pi/(2\sqrt{m}f_n)]}. \tag{22}$$

Note that when f_n approaches $1/\sqrt{m}$, the limit of gain M is infinity, as it is the resonant frequency of L_m, L_r, and C_r. In practice, the operation region of the LLC converter is set in the ZVS zone and the frequency range is above $\sqrt{m}$. If input voltage exceeds the limit, the converter will be unable to maintain the required output level under zero-load condition. Instead, the output voltage will become

$$V_o = \frac{m-1}{m\cos[\pi/(2\sqrt{m}f_n)]} \frac{V_{in}}{n}. \tag{23}$$

V. Peak Gain Approximation

From mode analysis, continuously decreasing switching frequency or increasing load will cause the resonant circuit to enter PN or PON mode from PO or NP mode, whereas the gain slows down its increase and eventually starts to drop. In other words, the peak gain only occurs in PN and PON modes. Since a peak gain point is also the ZCS/ZVS boundary [1], the resonant tank current i_r crosses zero at the instants when switches turn ON/OFF, and that is

$$i_{rPn}(0) = i_{rNn}(\theta_N) = 0. \tag{24}$$

From the symmetry condition $v_{CPn}(0) = -v_{CNn}(\theta_N)$, which applies to both PON and PN modes, the peak gain expression can be derived as

$$M_{pk} = \frac{2}{I_{rPn} - I_{rNn}}. \tag{25}$$

For PN mode, after properly manipulating (9) and (24), we arrive at

$$I_{rPn} = \frac{\pi}{2(m-1)f_n \sin\theta_P}, \quad I_{rNn} = \frac{\pi}{2(m-1)f_n \sin\theta_N} \tag{26}$$

where

$$\theta_P = \frac{1}{2}\left[\frac{\pi}{f_n} + \cos^{-1}\left(\cos\frac{\pi}{f_n} - \frac{\pi}{2(m-1)f_n}\sin\frac{\pi}{f_n}\right)\right]$$
$$\theta_N = \frac{1}{2}\left[\frac{\pi}{f_n} - \cos^{-1}\left(\cos\frac{\pi}{f_n} - \frac{\pi}{2(m-1)f_n}\sin\frac{\pi}{f_n}\right)\right].$$

Therefore, the peak gain has a closed-form expression by substituting (26) into (25), which is a function of m and f_n. In PN mode, the converter reaches the peak gain point under relatively heavy-load condition and the corresponding operation frequency is close to resonant frequency f_r. The load power at the peak gain point can be derived from (9), which is

$$p_{on} = \frac{1}{2(m-1)}\left(\tan\frac{\theta_P}{2} - \tan\frac{\theta_N}{2}\right). \tag{27}$$

A gain curve with lighter load condition has a higher peak value and lower peak gain frequency, and therefore the peak point may move into PON mode. The current parameters I_{rPn} and I_{rNn} can be derived from the peak gain condition (24) and boundary equations obtained by applying (4)–(8) to PON mode, and we can have

$$I_{rPn} = \sqrt{(I_{rOn}\sin\theta_{O0})^2 + (\sqrt{m}I_{rOn}\cos\theta_{O0} - 1)^2}$$
$$I_{rNn} = \sqrt{I_{rOn}^2 - 1/(m-1)}. \tag{28}$$

Also, the load power at the peak gain can be derived as follows:

$$p_{on} = \frac{f_n}{\pi}\left[\frac{m-1}{2}(I_{rOn}\cos\theta_{O0})^2 - \sqrt{m}I_{rOn}\cos\theta_{O0} + \sqrt{(I_{rOn}\sin\theta_{O0})^2 + (\sqrt{m}I_{rOn}\cos\theta_{O0}-1)^2} - \sqrt{I_{rOn}^2 - \frac{1}{m-1}} + \frac{m}{2(m-1)}\right]. \quad (29)$$

Expressions (28) and (29) are functions of I_{rOn} and θ_{O0}, but they have no further explicit forms. MATLAB is used to find the numerical solutions of the peak gain equations given m and f_n values. From the frequency-sweep results, it is observed that I_{rOn} is proportional to f_n, which decreases as f_n goes down. To simplify the calculation, we make the assumption that I_{rOn} is a linear function of f_n. There are two peak gain points where I_{rOn} can be solved and used to determine the linear approximation function. One is at the boundary between PON and PN mode, whereas the other is under zero-load condition.

Although at the PN/PON boundary the converter operates in PN mode and there is no stage O in the half cycle, the PON mode equations still apply by letting $\theta_O = 0$. The boundary stage O current magnitude I_{rOnb} can be solved as follows:

$$I_{rOnb} = \frac{1}{m-1}\sqrt{\left(\frac{\pi}{2f_{nb}}\right)^2 + m} \quad (30)$$

where f_{nb} denotes the boundary frequency of PN/PON. To solve f_{nb}, applying the boundary condition between PON and PN mode (13) and peak gain condition (24) to PN mode equations (9) yields that

$$\tan\left(\frac{\pi}{f_{nb}}\right) = \frac{m-1}{(2m-1)\frac{f_{nb}}{\pi} + \frac{\pi}{4f_{nb}}} \quad (31)$$

which is a transcendental equation of f_{nb} and thus has no closed-form solution. However, it can be numerically estimated using curve-fitting technique. It is observed that f_{nb} tends to become smaller when m increases; as m approaches infinity, the limit of f_{nb} is 0.735; as m approaches infinity, the limit of f_{nb} is 1. Hence, the boundary frequency f_{nb} is evaluated as follows:

$$f_{nb} = f_{nb\_\min} + (1 - f_{nb\_\min})/m^{1.11} \quad (32)$$

where $f_{nb\_\min} = 0.735$ is the lower limit of the frequency and the exponent of m, 1.11, is obtained from curve fitting.

Under zero-load condition, the LLC operates in O mode. Applying the boundary condition (5) to PON mode, we have

$$\frac{m-1}{\sqrt{m}}I_{rOn}\cos(\theta_O/\sqrt{m} + \theta_{O0}) = -1. \quad (33)$$

As the load is dropping to zero, stage O will span the whole half cycle and thus θ_O is equal to π/f_n. Since the ZVS/ZCS boundary condition requires that i_r initial value is 0, the initial phase angle θ_{O0} is also 0 under zero-load condition. Substituting $\theta_{O0} = 0$ into (33) and O mode symmetry conditions defined by (7), we can solve

$$I_{rOn0} = \sqrt{m}/(m-1)$$
$$f_{n0} = 1/\sqrt{m} \quad (34)$$

where I_{rOn0}, f_{n0} are the resonant current magnitude and frequency at zero load, respectively.

Therefore, the linear approximation function of I_{rOn} can be expressed as

$$I_{rOn}(f_n) = (I_{rOn0} - I_{rOnb})\frac{f_n - f_{nb}}{f_{n0} - f_{nb}} + I_{rOnb}. \quad (35)$$

After knowing I_{rOn}, the end-stage phase angle of the current i_{rOn} denoted as β can be solved from (33) as

$$\beta = \frac{\theta_O}{\sqrt{m}} + \theta_{O0} = \arccos\left(-\frac{\sqrt{m}}{(m-1)I_{rOn}}\right). \quad (36)$$

After proper manipulation of the boundary conditions, we arrive at an equation about θ_{O0} and β as

$$\cos(\beta)\theta_{O0} + \sin(\theta_{O0}) + \cos(\beta)\left(\frac{\pi}{f_n\sqrt{m}} - \beta\right) + \sin(\beta) = 0. \quad (37)$$

We use the Newton–Raphson method to estimate the initial phase angle θ_{O0}, which is given by

$$\theta_{O0} = \frac{\cos(\alpha)\alpha - \sin(\alpha) - \cos(\beta)\left(\frac{\pi}{f_n\sqrt{m}} - \beta\right) - \sin(\beta)}{\cos(\alpha) + \cos(\beta)} \quad (38)$$

where

$$\alpha = \frac{-1 - \cos(\beta)((\pi/f_n\sqrt{m}) - \beta) - \sin(\beta)}{\cos(\beta)}.$$

Hence, the peak gain points in PON mode can be directly calculated by applying (38), (35) to (28) and (29). Fig. 6 shows the comparison of the peak gains calculated by the approximation method and simulation. Note that the simulation only shows the peak gain results in PON mode, since in PN mode the peak gain has an exact solution given by (25), (26). It can be seen that the approximation matches the simulation. For a lighter load condition, the LLC converter can achieve higher peak gain at a lower switching frequency, and the peak gain decreases as the inductor ratio m increases.

VI. Experiment

To verify the mode analysis, an experimental full-bridge LLC converter prototype with 150 W, 210 V output has been built. The resonant frequency is set to 140 kHz with L_r as 3.9 μH and C_r as 330 nF. The magnetizing inductor L_m is set to 11 μH and thus m is 3.82. The transformer turns ratio n is 10/70. The experiment waveforms are given in Fig. 7 showing the resonant and output current waveforms in PO, PON, and OPO modes.

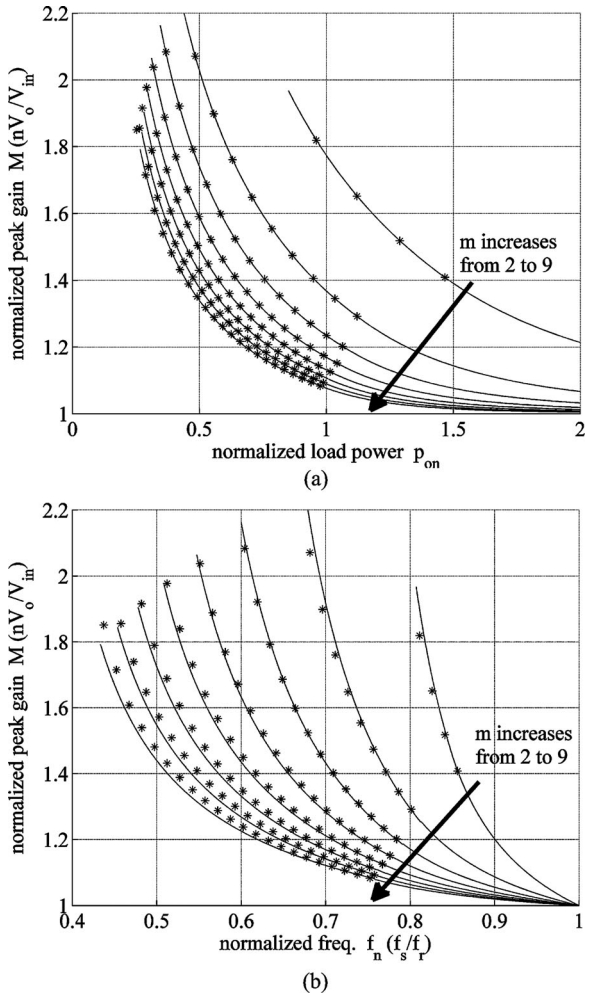

Fig. 6. Comparison between proposed approximation method (solid lines) and simulation result (markers) under various m. (a) Peak gain versus load. (b) Peak gain versus frequency.

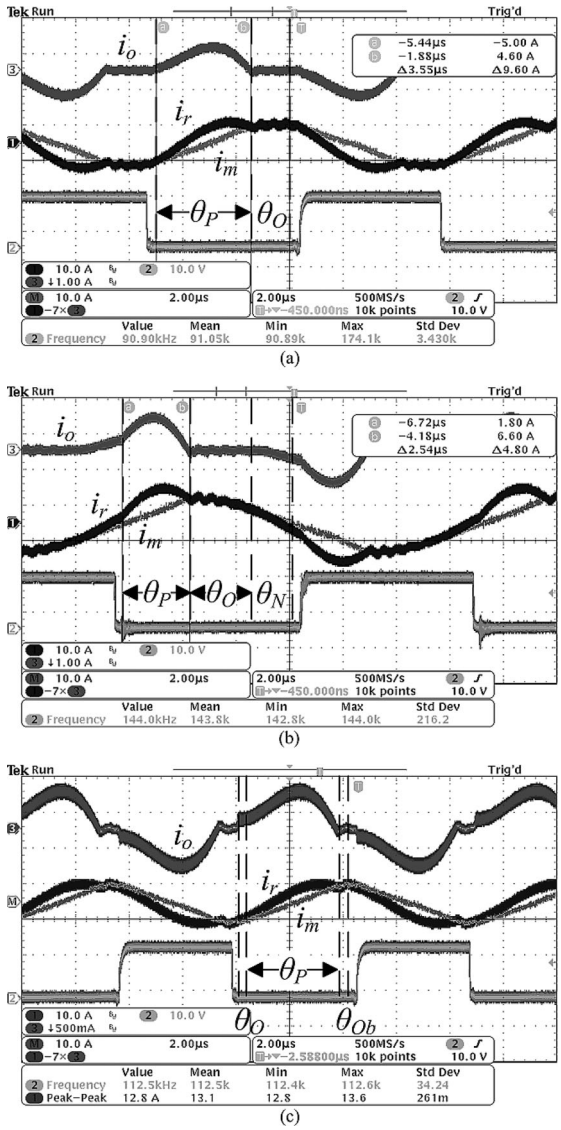

Fig. 7. Experimental waveforms (Ch1: i_r, Ch2: Q2 driving signal, Ch3: i_o, ChM: i_m). (a) PO mode: $P_o = 60$ W, $V_{\rm in} = 17.7$ V, $V_o = 212$ V, $f_s = 90.9$ kHz. (b) PON mode: $P_o = 60$ W, $V_{\rm in} = 10.4$ V, $V_o = 215$ V, $f_s = 74.5$ kHz. (c) OPO mode: $P_o = 60$ W, $V_{\rm in} = 26.8$ V, $V_o = 210$ V, $f_s = 112.5$ kHz.

When Q2 driving signal decreases, Q2, Q4 are OFF and Q1, Q3 are ON, which is the half cycle that the previous analysis and discussion are focused on. For the whole switching cycle, it can be seen that the current waveforms in one half cycle are turned upside-down compared to the other half. The current i_o shown in Fig. 7 is equal to $n(i_r - i_m)$, and therefore, it remains zero in stage O and is positive in stage P and negative in stage N. The waveforms are in good agreement with the mode analysis. The gain characteristic curves are shown in Fig. 8. The comparison shows that the gain prediction from mode equations has much higher accuracy than FHA. When the switching frequency is close to f_r, the gains obtained from FHA are almost the same as the ones solved from mode analysis. However, if the operation frequency changes farther away from f_r, the gain difference from two methods tends to become larger. For a wide input voltage range, FHA fails to provide an accurate gain prediction. Also, the estimated peak gains trajectory in Fig. 8 crosses the measured peak points closely, which verifies the effectiveness of the approximation method.

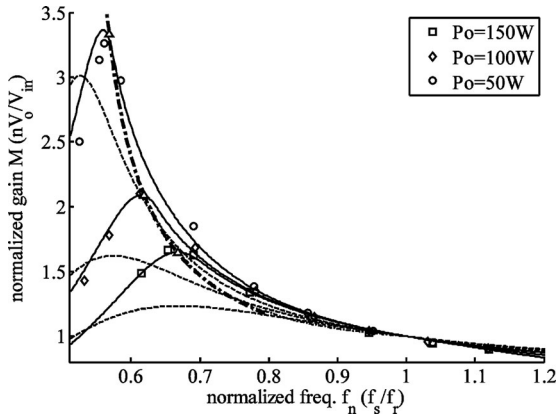

Fig. 8. Gain curves obtained from mode analysis (solid lines), FHA (dashed lines), experiment (markers), and estimated peak gain trajectory (dashed–dotted lines) with "Δ" markers showing the estimated peak gain points at corresponding loads.

VII. Conclusion

A generalized analysis of the operation modes of the LLC converter is presented. Based on the voltage and current behavior of the resonant tank, the converter's operation is summarized and divided into three resonant stages. Different operation modes consist of different combinations of the three stages, and six modes are analyzed. For each mode, the mode equations are derived from the current and voltage boundary conditions between stages to describe the circuit behavior and solve for the dc gain. The mode boundaries and distribution under various loads and switching frequencies are studied. From the mode analysis, an approximation method for peak gain estimation is developed, which simplifies the calculation of peak gain and the related load power values and demonstrates high accuracy. The theoretical analysis and the estimation method are verified by experimental results.

References

[1] B. Yang, F. C. Lee, A. J. Zhang, and G. Huang, "LLC resonant converter for front end DC/DC conversion," in *Proc. IEEE Appl. Power Electron. Conf. Expo*., 2002, pp. 1108–1112.

[2] W.-Y. Choi, J.-M. Kwon, and B.-H. Kwon, "High-performance front-end rectifier system for telecommunication power supplies," in *Proc. Inst. Elect. Eng*., Jul. 2006, vol. 153, no. 4, pp. 473–482.

[3] R. Beiranvand, B. Rashidian, M. R. Zolghadri, and S. M. H. Alavi, "Designing an adjustable wide range regulated current source," *IEEE Trans. Power Electron*., vol. 25, no. 1, pp. 197–208, Jan. 2010.

[4] M. S. Almardy and A. K. S. Bhat, "Three-Phase (LC)(L)-type series-resonant converter with capacitive output filter," *IEEE Trans. Power Electron*., vol. 26, no. 4, pp. 1172–1183, Apr. 2011.

[5] Y. Gu, Z. Lu, L. Hang, Z. Qian, and G. Huang, "Three-level LLC series resonant DC/DC converter," *IEEE Trans. Power Electron*., vol. 20, no. 4, pp. 781–789, Jul. 2005.

[6] B. Yang, R. Chen, and F. C. Lee, "Integrated magnetic for LLC resonant converter," in *Proc. IEEE Appl. Power Electron. Conf. Expo*., 2002, vol. 1, pp. 346–351.

[7] A. K. S. Bhat, "Analysis and design of LCL-type series resonant converter," *IEEE Trans. Ind. Appl*., vol. 41, no. 1, pp. 118–124, Feb. 1994.

[8] R. L. Steigerwald, "A comparison of half-bridge resonant converter topologies," *IEEE Trans. Power Electron*., vol. 3, no. 2, pp. 174–182, Apr. 1988.

[9] A. K. S. Bhat, "A generalized steady-state analysis of resonant converters using two-port model and Fourier-series approach," *IEEE Trans. Power Electron*., vol. 13, no. 1, pp. 142–151, Jan. 1998.

[10] A. J. Forsyth, G. A. Ward, and S. V. Mollov, "Extended fundamental frequency analysis of the LCC resonant converter," *IEEE Trans. Power Electron*., vol. 18, no. 6, pp. 1286–1292, Nov. 2003.

[11] B. Lee, M. Kim, C. Kim, K. Park, and G. Moon, "Analysis of LLC resonant converter considering effects of parasitic components," in *Proc. IEEE Int. Telecommun. Energy Conf*., Oct. 2009, pp. 1–6.

[12] I. Batarseh, R. Liu, A. Ortiz-Conde, A. Yacoub, and K. Siri, "Steady state analysis and performance characteristics of the LLC-type parallel resonant converter," in *Proc. IEEE Power Electron. Spec. Conf. Rec*., Jun. 1994, pp. 597–606.

[13] I. Batarseh, "State-plane approach for the analysis of half-bridge parallel resonant converters," in *Proc. Inst. Elect. Eng*., Jun. 1995, vol. 142, no. 3, pp. 200–204.

[14] N. H. Kutkut, C. Q. Lee, and I. Batarseh, "A generalized program for extracting the control characteristics of resonant converters via the state-plane diagram," *IEEE Trans. Power Electron*., vol. 13, no. 1, pp. 58–66, Jan. 1998.

[15] M. Vuksic, S. M. Beros, and L. Vuksic, "The multiresonant converter steady-state analysis based on dominant resonant process," *IEEE Trans. Power Electron*., vol. 26, no. 5, pp. 1452–1468, May 2011.

[16] J. H. Cheng and A. F. Witulski, "Analytic solutions for LLCC parallel resonant converter simplify use of two-and three-element converters," *IEEE Trans. Power Electron*., vol. 13, no. 2, pp. 235–243, Mar. 1998.

[17] J. F. Lazar and R. Martinelli, "Steady-state analysis of the LLC series resonant converter," in *Proc. IEEE Appl. Power Electron. Conf. Expo*., 2001, vol. 2, pp. 728–735.

[18] C. Oeder, A. Bucher, J. Stahl, and T. Duerbaum, "A comparison of different design methods for the multiresonant LLC converter with capacitive output filter," in *Proc. IEEE Control and Modeling for Power Electrnoics Conf*., Jun. 2010, pp. 1–7.

[19] M. P. Foster, C. R. Gould, A. J. Gilbert, D. A. Stone, and C. M. Bingham, "Analysis of CLL voltage-output resonant converters using describing functions," *IEEE Trans. Power Electron*., vol. 23, pp. 1772–1781, Jul. 2008.

[20] G. Ivensky, S. Bronshtein, and A. Abramovitz, "Approximate analysis of resonant LLC DC–DC converter," *IEEE Trans. Power Electron*., vol. 26, no. 11, pp. 3274–3284, 2011.

[21] B. Lu, W. Liu, Y. Liang, F. C. Lee, and J. D. van Wyk, "Optimal design methodology for LLC resonant converter," in *Proc. IEEE Appl. Power Electron. Conf. Expo*., 2006, vol. 2, pp. 533–538.

[22] R. Beiranvand, B. Rashidian, M. R. Zolghadri, and S. M. H. Alavi, "Optimizing the normalized dead-time and maximum switching frequency of a wide-adjustable-range LLC resonant converter," *IEEE Trans. Power Electron*., vol. 26, no. 2, pp. 462–472, Feb. 2011.

[23] B.-C. Kim, K.-B. Park, C.-E. Kim, B.-H. Lee, and G.-W. Moon, "LLC resonant converter with adaptive link-voltage variation for a high-power-density adapter," *IEEE Trans. Power Electron*., vol. 25, no. 9, pp. 2248–2252, Sep. 2010.

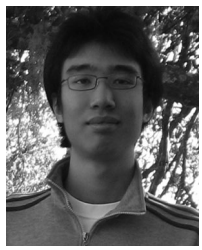

Xiang Fang (S'11) received the B.S. degree in electrical engineering from Tsinghua University, Beijing, China, in 2007. He is curently working toward the Ph.D. degree in power electronics from the University of Central Florida, Orlando.

He is a Research Assistant with Florida Power Electronicas Center, University of Central Florida, where he is involved in the modeling and design of dc/dc resonant converters. His research interests include renewable energy conversion, dc/dc conversion, and resonant power conversion.

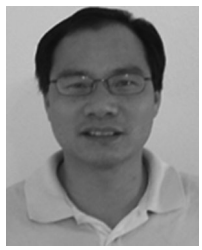

Haibing Hu (M'09) received the B.S. degree from the Hunan University of Technology, Hunan, China, in 1995, and the M.S. and Ph.D. degrees in electrical engineering from Zhejiang University, Zhejiang, China, in 2003 and 2007, respectively.

From 2007 to 2009, he was an Assistant Professor in the Department of Control Engineering, Nanjing University of Aeronautics and Astronautics, Nanjing, China, where he is currently an Associate Professor. In 2009, he joined the Department of Electrical Engineering, University of Central Florida, as a Postdoctoral Research Fellow. His research interests include digital control in power electronics, multilevel inverter, digital control system integration for power electronics and applying power electronics to distributed energy systems, and power quality. He has authored or coauthored more than 30 technical papers published in journals and conference proceedings.

Z. John Shen (S'90–M'94–SM'02–F'11) received the B.S. degree in electrical engineering from Tsinghua University, Beijing, China, in 1987, and the M.S. and Ph.D. degrees in electrical engineering from Rensselaer Polytechnic Institute, Troy, NY, in 1991 and 1994, respectively.

Between 1994 and 1999, he held a number of technical positions, including Senior Principal Staff Scientist with Motorola Semiconductor Products Sector, Phoenix, AZ. Between 1999 and 2004, he was with the University of Michigan-Dearborn, Dearborn. Since 2004, he has been with the University of Central Florida, Orlando, where he is currently a Professor of electrical engineering, the Director of the Power Semiconductor Research Laboratory, and the Associate Director of Florida Power Electronics Center. His current research interests include power semiconductor devices and integrated circuits, power electronics, automotive electronics, nanotechnology, and renewable-energy systems. He has authored or coauthored more than 100 journal and referred conference publications. He is the holder of 12 issued and several pending or provisional U.S. patents. He is the inventor of the world's first submilliohm power metal–oxide–semiconductor field-effect transistor.

Dr. Shen served as an Associate Editor of the IEEE TRANSACTIONSON ON POWER ELECTRONICS between 2006 and 2009. He served as the Technical Program Chair of the second IEEE Energy Conversion Congress and Expo in 2010, the 38th IEEE Power Electronics Specialists Conference in 2007, and the first IEEE Vehicle Power and Propulsion Conference in 2005. He currently serves as the Vice President of Products of the IEEE Power Electronics Society. He has also served on numerous IEEE conference and workshop organizing committees, and international editorial boards. He is a recipient of the 2003 U.S. National Science Foundation CAREER Award, the 2006 Transaction Prize Paper Award of the IEEE TRANSACTIONSON ON POWER ELECTRONICS from the IEEE Power Electronics Society, the 2003 IEEE Best Automotive Electronics Paper Award from the IEEE TRANSACTIONSONS ON VEHICULAR TECHNOLOGY, and the 1996 Motorola Science and Technology Award.

Issa Batarseh (F'06) received the B.S.E.E. degree in electrical and computer engineering, and the M.S. and Ph.D. degrees in electrical engineering, in 1983, 1985, and 1990, respectively, all from the University of Illinois, Chicago.

He is currently a Professor of electrical engineering with the School of Electrical Engineering and Computer Science, University of Central Florida (UCF), Orlando. From 1989 to 1990, he was a Visiting Assistant Professor with Purdue University, Calumet, IN, before joining the Department of Electrical and Computer Engineering, UCF, in 1991. His research interests include power electronics, developing high-frequency energy conversion systems to improve power density, efficiency, and performance, the analysis and design of high-frequency solar and wind energy conversion topologies, and power factor correction techniques. He is the author or coauthor of more than 60 refereed journals and 300 conference papers in addition to 14 U.S. patents. He is also an author of a textbook entitled *Power Electronic Circuits* (New York: Wiley, 2003).

Dr. Batarseh is a Registered Professional Engineer in the State of Florida and a Fellow Member of the IEE. He served as a Chairman for IEEE PESC'07 conference and was the Chair of the IEEE Power Engineering Chapter, and the IEEE Orlando Section.